Manipulating Quantum Interference Between σ and π Orbitals in Single Molecule Junctions via Chemical Substitution and Environmental Control

*Hannah E. Skipper [a], Brent Lawson [b], Xiaoyun Pan [a], Vera Degtiareva [b], and Maria Kamenetska [a,b,c]**

[a] Department of Chemistry, Boston University, Boston, Massachusetts 02215, United States

[b] Department of Physics, Boston University, Boston, Massachusetts 02215, United States

[c] Division of Material Science and Engineering, Boston University, Boston, Massachusetts, 02215, United States

KEYWORDS

Quantum interference, single-molecule conductance, nanoscale contacts, electron transport, electronic structure, molecular switches

ABSTRACT

Understanding and manipulating quantum interference (QI) effects in single molecule junction conductance can enable design of molecular-scale devices. Here we demonstrate QI between σ and π molecular orbitals in a ~ 4 Å molecule, pyrazine, bridging source and drain electrodes. Using single molecule conductance measurements, first principles analysis and electronic transport calculations, we show that this phenomenon leads to distinct patterns of electron transport in nanoscale junctions, such as destructive interference through the para position of a six-membered ring. These QI effects can be tuned to allow conductance switching using

environmental pH control. Our work lays out a conceptual framework for engineering QI features in short molecular systems through synthetic and external manipulation that tunes the energies and symmetries of the σ and π channels.

Quantum interference (QI) in nanoscale contacts can be harnessed to enable functional electronic phenomena in next generation electronic devices. In molecular circuits, QI has been shown to affect the conductance of a metal-molecule-metal junction, suggesting that controlled manipulation of QI can enable toggling of the conducting state from on to off.[1-4] Recent work has demonstrated mechanosensitive QI phenomena in molecular junctions, which result in variations in conductance during mechanical modulation experiments.[5-8] Other strategies to tune QI in molecular junctions include synthetic modifications of the molecule and use of environmental stimuli such as electrode potential and cation-gating mechanisms.[9-14] QI results from electrons tunneling across two or more electronic states in the molecular junction. These states derive from molecular orbitals (MOs) which impart distinct phases to the tunneling electrons at the Fermi energy. MOs are either π or σ—antisymmetric or symmetric relative to the internuclear axis of the molecule, respectively. Until now, all observed interference effects have been derived from π-π or σ-σ MO interactions. The reliance on orbitals with similar symmetry, like all π or all σ, limits the range of accessible QI phenomena. For example, most reported trends and modulation of destructive quantum interference (DQI) involve the π system of extended conjugated systems because the more conducting π system of these molecules dominates transport. In π orbital-mediated interference, para-linked species, which also bind more efficiently due to steric interactions, are better conducting than meta-linked analogues. The presence of numerous frontier π-orbitals in large conjugated systems means that the on/off conductance ratio in these extended

molecular systems is limited. In shorter, often saturated molecules, interference between σ channels has also been observed, but complete DQI where conductance is fully suppressed is rare in organic systems.[15, 16]

Here we demonstrate that QI between the π and σ channels can be harnessed in sub-nanometer molecules to create junctions with adjustable interference phenomena with a high on/off ratio. We use the simple 6-member conjugated ring molecules to demonstrate that synthetic substitution can reorder the relative energies of σ and π MOs and introduce QI between these transport channels. We demonstrate how single atom substitutions from carbon to nitrogen in the para position of benzene to yield pyrazine, shown in Figure 1A, creates a tunable and synthetically accessible molecular framework for QI manipulation and environmental control. First, through experiment, analysis and density functional theory calculations, we show that interference between σ and π channels determines transport in pyrazine. We demonstrate suppression of conductance through the para channel of this molecule which is only possible through σ-π DQI. Then, by synthetically tuning the relative energy and symmetry between these MOs we adjust the QI phenomena through the molecule. Finally, we show experimentally and validate computationally that recovery of the conductance signal can be observed through environmental pH control. This work is an unambiguous demonstration of QI environmental manipulation in a molecule shorter than ~ 4 Å and with a constructive QI (CQI) conductance as high as benzene at ~1% of a fully open quantum channel. Importantly, the restricted set of binding degrees of freedom that is characteristic of short molecular junctions allows us to achieve high on/off ratios between states of the molecular circuit through environmental control.

RESULTS AND DISCUSSION

Both benzene and pyrazine (pyz), shown in Figure 1A, are 6-membered conjugated rings, but whereas benzene is composed of all sp^2 carbons, pyz contains two nitrogen atoms in the 1 and 4 (para) positions. Benzene-based bridges, such as 1,4-benzenediamine shown in the middle column in Figure 1A are well-studied systems with a high molecular conductance approaching ~1% of $1G_0$, which depends slightly on the chemical linker used to bind it to Au electrodes.[17, 18] Transport through these molecules is known to strongly dependent on the position of the linker electrode contacts due to QI effects, with para and meta substitution resulting in CQI and DQI respectively.[2, 11, 19]

Pyridine-type nitrogen atoms are robust and selective linker groups for binding to Au electrodes, suggesting pyz which contains two pyridine N atoms in the para position of a six-membered ring, is an ideal candidate for junction bridging.[20] Yet few reports of pyrazine conductance are found in the literature and our own measurements show no discernible signal as we show further below.[21, 22] We reason that the absence of a reliable pyrazine conductance signature is due to the reordering of frontier MOs in pyz compared to benzene as shown in Figure 1A, left column. The highest occupied molecular orbital (HOMO) and lowest unoccupied molecular orbital (LUMO) of benzene consist of two degenerate MOs that all have π character. In benzene-based bridges, these π -based frontier MOs dominate transport at the Fermi energy (E_F), resulting in CQI through para- and DQI through meta-linked molecules.[11, 19] In contrast, in pyz, the HOMO is σ dominated and the LUMO retains the π character of the benzene LUMO. The rest of the π-based MOs in pyz are shifted away from E_F to the LUMO+1, HOMO-1 and HOMO-3 (Figure 1A, right column). MOs with nodes in the 1 and 4 positions where the molecule binds to

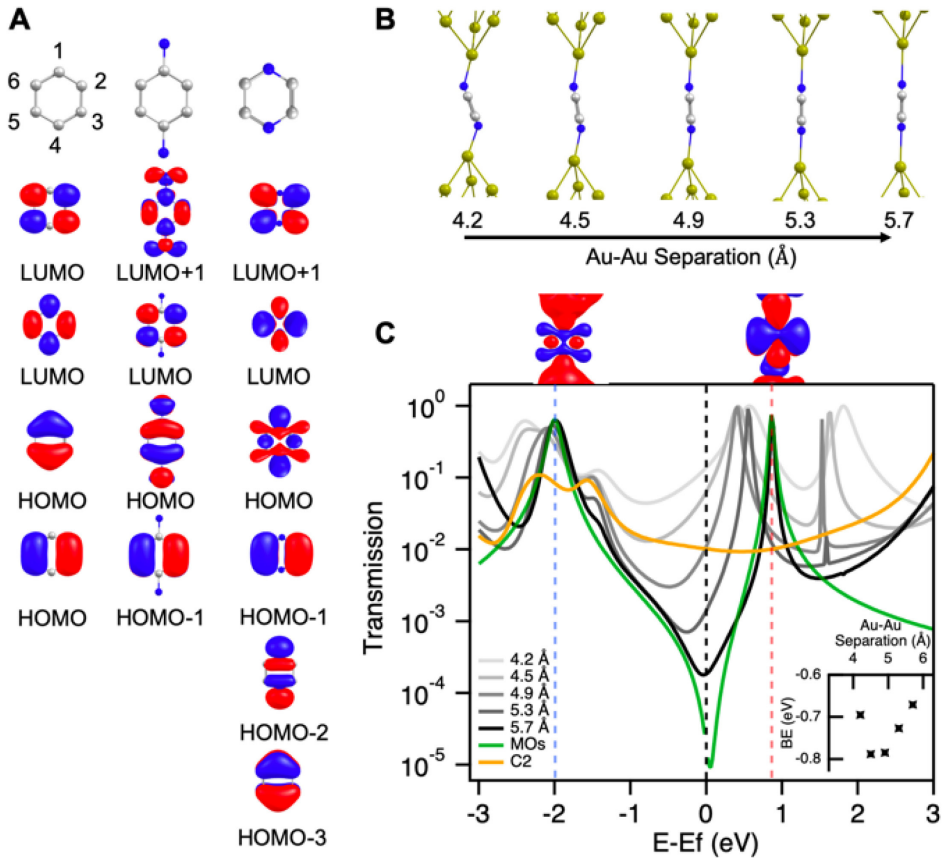

Figure 1. A) Frontier MOs of benzene (left), 1,4-benzenediamine (middle) and pyz (right) at B3LYP/Def2-TZVP level of theory. B) Relaxed geometries of pyz junctions at various junction extensions with Au37 electrodes. Au-Au separation is reported from edge to edge of the apex Au atoms. C) Transmission spectra and binding energy (BE) per Au-N bond (inset) of pyz at various junction lengths. Transmission calculated as $T = |t_{HOMO} + t_{LUMO}|^2$at 5.7 Å Au-Au separation (green trace). The black vertical dashed line indicates the Fermi energy (E_F). Isosurface plots of the molecular orbitals in the 5.7 Å junction at -2.0 eV (HOMO) and 0.9 eV (LUMO) are shown above and indicated by the blue and red dashed lines respectively. Transmission of 1,2-diaminoethane (yellow trace).

the electrodes, such as the pyz HOMO-1, will not contribute to transport through the para channel. Thus, we predict that transport in pyz will be dominated by the σ HOMO and the π LUMO. Transport at E_F can then be approximated as the modulus squared of the sum of the individual transmission coefficients.[2]

$$T = |t_\sigma + t_\pi|^2 = |t_\sigma|^2 + |t_\pi|^2 + 2Re(t_\sigma^* t_\pi) \quad (1)$$

Equation 1 is a general description of coherent transmission through two resonances, t_σ and t_π. In the case considered here, the σ and π orbitals are on a single molecule and the injection occurs at a single binding attachment spot, so the transmission is coherent and Equation 1 is applicable. The last term on the right of Equation 1 is the QI contribution between the two channels. Usually, σ and π channels do not both contribute to conductance or to QI. In conjugated systems, typically $t_\pi \gg t_\sigma$ and the π channel dominates the transmission. In saturated systems, only the σ channel is available. However, in a conjugated molecule as short as pyz, the σ and π transport channels are of similar amplitude. The conductance of saturated and conjugated molecules which are ~0.5 nm long, for example 1, 2- ethylenediamine and 1,4-benzenediamine has been determined to be ~10^{-2} G_0 in both cases.[17, 18, 23] In other words, we can assume that in pyz, $t_\pi \approx t_\sigma$ so that the interference term can be pronounced.[15, 24] Since the phase change in the HOMO and LUMO between the 1 and 4 positions is the same in Figure 1A, the *overall* phase difference between t_π and t_σ at E_F will be π (180˚) assuming there is no tilting of the molecule relative to gold electrodes. In this situation, the last term of Equation 1 becomes negative and it predicts DQI through the para channel.[2]

We now turn to density functional theory (DFT) and non-equilibrium Green's Function (NEGF) transmission calculations of realistic pyz junction geometries.[25, 26] The pyz molecule is relaxed with Au37 electrodes, which are frozen except for the four apex Au atoms on each

electrode (see methods for more details). Each Au electrode is moved in or out in increments of 0.05 Å. At each step, the junction geometry is relaxed and the binding energy and the transmission is calculated as detailed in the methods. A selection of relaxed junction geometries with increasing electrode distances from left to right are shown in Figure 1B (see Figure S1 for all geometries). Figure 1C reports the transmission spectra and binding energy per Au-linker bond (inset) of pyz junctions over various Au-Au displacements. We note that no correction to the DFT-calculated HOMO-LUMO gaps has been applied, so they are underestimated here, but the overall transport trends and symmetry arguments are representative and meaningful.[27] As shown in Figure 1B, at shorter junction lengths, the pyz molecule tilts to fit in the junction. These tilted geometries have a relative high transmission at E_F (indicated by the dashed black line), approximately 5 x 10^{-2} G_0 for the 4.5 Å geometry measured from edge to edge of the apex Au atoms, as shown by the lighter gray traces in Figure 1C. In these configurations, the LUMO peak at ~ 0.9 eV has more overlap at the E_F than the HOMO peak. We also see an emergent gateway state at ~ -1.5 eV which has a low amplitude and does not contribute significantly to conductance at Fermi.[28-30] From Figure 1A, we infer that the empty part of the spectrum is dominated by the π system. When the molecule is tilted, the π LUMO couples effectively to Au, resulting in broader LUMO resonance with a large overlap at E_F; $t_\pi \gg t_\sigma$ and transport is LUMO dominated at shorter junction lengths (< 5 Å). We note that in this tilted confirmation, when the Au electrodes bind to the opposite sides of the π system, the QI between σ and π is expected to be constructive because of the extra phase change in π MOs across the internuclear axis. In experiments, the typical Au-Au edge-to-edge distances exceed 5 Å so we do not expect these short geometries to dominate measurements of single molecule conductance.[31-33]

As the junction is elongated, the lone pairs of the N atoms, which are part of the σ framework, couple to the electrodes and the pyz molecule binds vertically in the junction (Figure 1B). In the transmission spectrum (Figure 1C) for the junction fully extended to 5.7 Å, neither the filled nor the empty part of the spectrum solely dominate transport at E_F. Instead, a typical DQI signature—a deep dip in the transmission spectrum—is observed around E_F and the transmission is lower by over 2 orders of magnitude, as shown by the solid black trace in Figure 1C. Isosurface plots of the 5.7 Å vertical junction geometry on top of Figure 1C show that the junction resonances closest to E_F in the filled (left) and empty (right) part of the spectrum have σ and π character, respectively.

We emphasize that the transport predicted for the fully stretched pyz at E_F is lower than of a typical sigma-conducting alkane of similar length, 1,2-diaminoethane, as shown in Figure 1C. Therefore, the low transmission of pyz cannot be explained by a suppression of the π channel only due to a lack of coupling in the vertical geometry.[15] Instead, we observe a situation where $t_\pi \approx t_\sigma$ and there is an overall phase change of π (180°) between the para positions in t_π and t_σ at the E_F.[2] Using Equation 1 and plugging in the values of the frontier resonance positions and width from fits to the black curve in Figure 1C, we obtain an approximate transmission. This is plotted in green in Figure 1C and has excellent qualitative agreement with the DFT and NEGF-calculated transmission of the vertical geometry. Therefore, we conclude that the DQI through the para channel of pyz in the vertical geometry is due to destructive interference between the σ and π channels, or HOMO and LUMO respectively.

We use single molecule conductance measurement to experimentally detect the QI effects through both the para and meta pathways of the pyz ring. We perform STMBJ measurements using a home-built instrument and protocol as previously described.[34, 35] Briefly, we bring Au electrodes

in and out of contact under a constant bias of 500 mV and record the conductance (current/voltage) during this junction-formation process. Conductance traces recorded during junction stretching show plateaus at integer values of G_0 which correspond to the formation of Au contacts with an integer number of Au atoms in the junction cross-section. Individual traces for clean Au are shown in the inset of Figure 2. Thousands of such conductance traces are compiled into histograms without data selection and normalized to enable comparison. An example of a clean Au histogram is shown in Figure 2 where a pronounced peak at $1G_0$ is evident. After the Au contact is broken, a nano-gap forms between the Au electrodes and a molecule present on the surface can bridge the Au electrodes to form a molecular junction with a conductance that is typically less than $1G_0$.

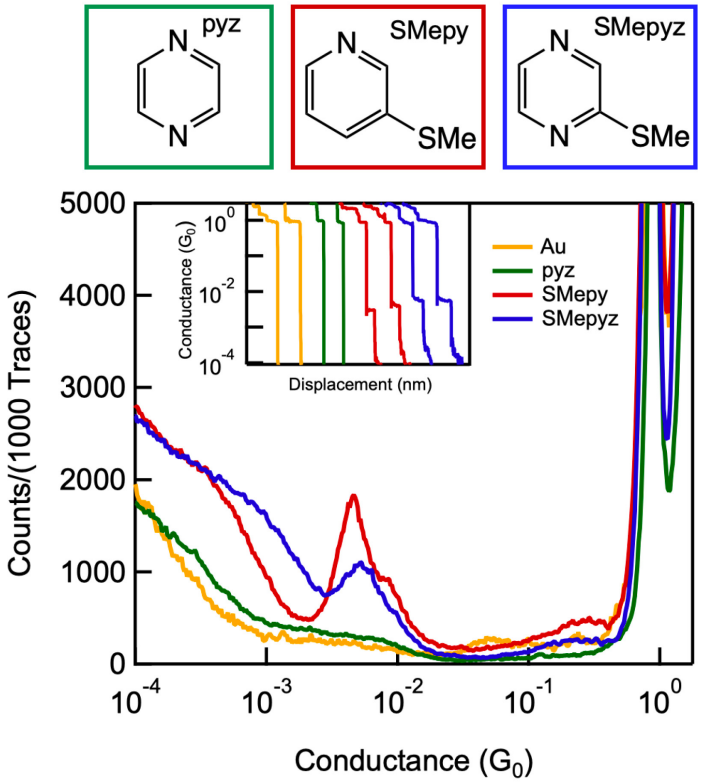

Figure 2. 1D conductance histogram of pyrazine (green), SMepy (red) and SMepyz (blue) at 1mM concentrations in TCB with a 500 mV bias. Example traces are shown in the inset and structures are shown above.

Figure 2 demonstrates the experimentally determined conductance signatures of pyz-based molecules with linker groups (pyridine N, or SMe) which allow selective bridging of Au electrodes to either the para (1,4) or the meta (1,3) positions.[20, 23, 36] We observe that pyz, with linkers only at the para position, does not produce clearly identifiable molecular conductance signatures as seen in the individual experiment traces (Figure 2 inset) and in the histogram (Figure 2) in green as predicted by our analysis above. Measurements performed at lower (100 mV) and higher (800 mV) bias reported in Figure S2 are consistent with 500 mV measurements in Figure 2. To eliminate the possibility that the pyz N atoms are not able to bind to Au, we perform measurements of 2-thiomethylpyridine (SMepy) and 2-thiomethylpyrazine (SMepyz) both of which have one SMe linker in the 3 positions. The traces and histograms are shown in Figure 2 in red and blue for SMepy and SMepyz respectively. For both molecules, we observe a clear conductance feature near 5×10^{-3} G_0, with a slight shoulder at higher conductance consistent with binding through pyridine linker groups.[20] Two-dimensional (2D) conductance histograms of pyz, SMepy and SMepyz, which display conductance as a function of electrode displacement are included in Figure S3. With pyz, we observe a steep conductance decay instead of a conductance plateau, which is in agreement with the DFT-predicted drop in conductance during junction elongation in Figure 1C. In contrast, with SMepy and SMepyz, clear conductance plateaus are present, corresponding to the peaks in Figure 2. We conclude that the pyrazine N is able to bind to Au and produce conductance plateaus when another linker group on the ring is present to bridge the junction. Importantly, for SMepyz, which contains both para (N-N) and meta (N-S) binding sites, we observe only a single conductance feature. The similarity in conductance values for SMepyz and SMepy indicates that transport in SMepyz occurs through the meta N-S pathway, rather than the para N-N pathway, of

the pyrazine ring. Conductance through quinazoline, which has a meta N-N rather than a para N-N pathway also occurs (Figure S4). Additionally, the calculated binding energies of the Au-N bonds in pyz are ~ 0.7 - 0.8 eV, comparable to other linker groups such as NH_2 and SMe, suggesting that pyz should bind in the Au junction (Figure 1C inset).[23, 37, 38] Therefore, we conclude that pyz, like SMepy and SMepyz, is able to bind to Au through the N atoms, but that the conductance through the N-N para channel is suppressed due to DQI as we predicted.

To summarize our results so far, we find that substituting pyridine N atoms into the para positions of a benzene ring leads to a rearrangement of MOs that results in distinct QI phenomena between the σ and π MOs. As a result, in pyz molecules, the para channel is non-conducting due to DQI. Interestingly, substitution at the 3 position with the SMe linker preserves the DQI through the 1,4 channel.

We perform calculations to understand the effect of π-donating substituents like SMe on the electronic structure of pyz derivatives and to gain insight into routes to turn on conductance through the para channel. We consider the effect of SMe as well as OH substituents, which can influence the electronic structure of pyz, but which are not known to bind to Au in break junction experiments.[39] The gas phase MOs of SMepyz and OHpyz are shown in Figure S5. Transport calculations are shown in Figure 3 for OHpyz and Figure S6 for SMepyz. We observe that the features of the two molecules are similar (Figure S6) and we focus on the OHpyz results in Figure 3 as representative for both. The HOMO in OHpyz has π symmetry while the σ MO is now the HOMO-1, which is the reverse of pyz. Furthermore, the π HOMO of OHpyz has non-zero weight on the N atoms and may contribute to transport through the para channel of OHpyz. The symmetries of the π HOMO and LUMO indicate that the relative phase between these MOs is zero at E_F and should result in CQI through the para pathway. We also note that the σ HOMO-1 retains

the symmetry of the HOMO of pyz and is only ~ 0.3 eV below the π HOMO and can interfere destructively with the π LUMO (Figure S5). To summarize this analysis, we predict that in OHpyz, three MOs contribute to transport at E_F through a combination of HOMO-LUMO CQI and HOMO-1-LUMO DQI.

To test these predictions, we now model the conductance of fully elongated geometries of OHpyz and the unsubstituted pyz shown in Figure 3B-C. These structures represent the junctions immediately before rupture (for more details see Figures S1, S6-S8). We observe that the transmission at E_F through the para pathway of OHpyz (gray) is higher than that of unsubstituted pyz (black) and the DQI feature in transmission at E_F is diminished. We conclude that the nearly degenerate HOMO and HOMO-1 of the gas-phase OHpyz both contribute to the broad peak in the filled part of the spectrum at ~ -2eV in Figure 3C. This is demonstrated by isosurface plots of the eigenchannels in Figure S9. Using Equation 1 and including the relative symmetries of the HOMO-1, HOMO and LUMO seen in Figure 3A, we reproduce a qualitatively similar transmission to the DFT calculated result in grey. This result is plotted in green in Figure 3C and suggests that QI effects between three MOs determine the conductance of OHpyz as we predicted. We note that in SMepyz transmission in Figure S6, the DQI feature is more pronounced than in OHpyz because the π-based HOMO has less weight on the N atoms and contributes less to CQI. Apparently, the inclusion of the OH group, and SMe to a lesser extent, in the meta position mitigates, but does not eliminate, the DQI through the para channel due to the reordering of frontier MOs as discussed above.

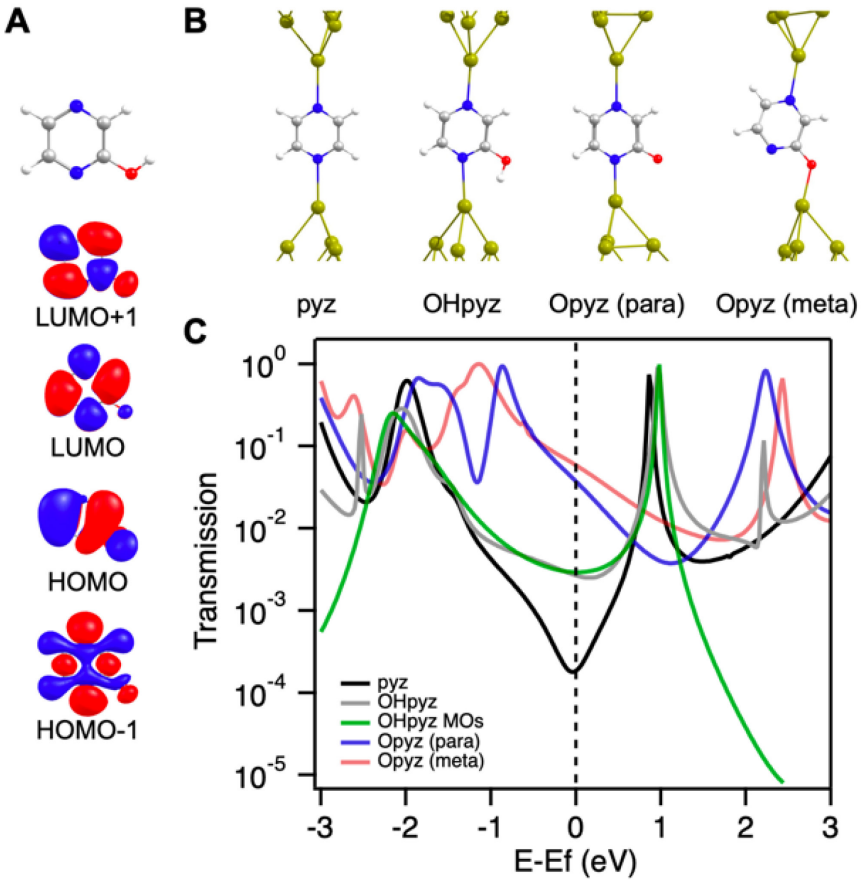

Figure 3. A) Frontier MOs of OHpyz at B3LYP/Def2-TZVP level of theory. B) Relaxed junction geometries from left to right of pyz, OHpyz, Opyz (para) and Opyz (meta) at the longest extension before Au rupture (5.7 Å, 5.3 Å, 5.1 Å and 5.5 Å respectively, measured from edge to edge of the apex Au atoms). C) Corresponding calculated transmission spectra for the pyz-based junction geometries shown above. Transmission calculated as $T = |t_{HOMO-1} + t_{HOMO} + t_{LUMO}|^2$ for OHpyz (green trace). The vertical dashed line indicates E_F.

To further modulate the QI, we deprotonate the OH group on the pyrazine ring and repeat the calculations of the vertical geometry and transmission as shown in Figure 3B (labeled Opyz para) and Figure 3C in blue. The HOMO and LUMO of the anion are shifted to higher energies as

expected for the anion relative to the neutral molecule, which also causes the DQI feature to shift to higher energies, leading to a significantly higher transmission at E_F compared to the neutral OHpyz (grey). Importantly, the DFT-predicted transport through the para Opyz is about one order of magnitude higher than the neutral OHpyz. The charged Opyz also binds to the electrodes more strongly than the neutral pyz or OHpyz, with binding energies of ~ 2 eV and ~ 0.8 eV per Au-N bond respectively (Figures S1, S6 and S7). DFT results suggest that binding through the O^- in the 3 position of the ring is also robust with a binding energy of ~ 2 eV (labeled Opyz meta in Figure 3B and Figure 10). From Figure 3C, we find that the transmission through the meta pathway (red) is higher at E_F than the para pathway (blue).

Overall, the DFT results suggest that conductance through OHpyz can be turned on through deprotonation of the OH substituent. To experimentally test this strategy, we perform single molecule conductance measurements of OHpyz at various pH according to established protocols.[35] The molecule exists in a tautomeric equilibrium between the enol (OH) and keto (=O) forms (Figure 4A). The conductance histogram from measurements recorded in the presence of OHpyz in neutral pH shown in Figure 4B (gray) produces a broad feature below 10^{-3} G_0. The feature is likely a result of dimer π-π stacking which has been widely reported in the literature.[5, 40, 41] Control measurements with 3-hydroxypyridine (OHpy) which lacks one binding site, but retains the conductance feature below 10^{-3} G_0 in Figure S10 (grey trace) support this conclusion.

We now experimentally measure conductance through deprotonated Opyz according to our established protocols.[35] We record single molecule conductance signatures through the Opyz molecule in basic conditions above pH 12 at both a 500 mV (Figure 4A) and 100 mV (Figure S12) bias. In this environment, two distinct conductance peaks appear in the histogram in Figure 4B: G1 at 8.3 x 10^{-3} G_0 (peak 1) and G2 at 2.6 x 10^{-3} G_0 (peak 2) with a G1/G2 conductance ratio of ~

3.2. Measurements of OHpyz in acidic conditions (pH ~ 3) do not have these conductance features, but the addition of 1M NaOH base to the experiment restores conductance signatures (Figure S11A-C). This reversibility under changing pH confirms that the molecule is binding in its deprotonated form. Furthermore, measurements of KOpyz salt in neutral water (Figure S11D), produce the same conductance signature as deprotonated OHpyz, confirming that the anion Opyz is binding in the junction. The distinct conductance features in basic conditions are also clearly visible in the 2D histogram, in Figure 4C and agree with DFT calculated displacements in Figure 1 and S7.

To assign these peaks to binding geometries, we first confirm that O^- can form bonds to gold in our junctions in basic pH. Prior measurements have documented the binding of O- to under-coordinated Au upon deprotonation of carboxyl groups via pH and electrochemical methods.[42-45] We measure the conductance of Opy (Figure S11) by dissolving OHpy into pH12 solution. The molecular signature shows a clear conductance peak in basic conditions. Notably, the conductance of Opy peak is similar to peak G1 of Opyz. Both show an additional higher shoulder at ~1.5 times the conductance of the main peak when measured in solution, consistent with binding through a pyridine moiety (Figures S10 and S11).

Based on these control measurements and transport calculated in Figure 3C, we assign the higher conducting peak G1 of Opyz to the meta (N-O) channel where the molecule is bound through the oxygen at the 3 position.[46] Peak G2 corresponds to binding through the para (N-N) pathway. Critically, this lower conductance peak occurs after additional pulling when the molecule can straighten in the junction, indicating that we have successfully turned on conductance through the para channel by inducing deprotonation of OHpyz through environmental pH.

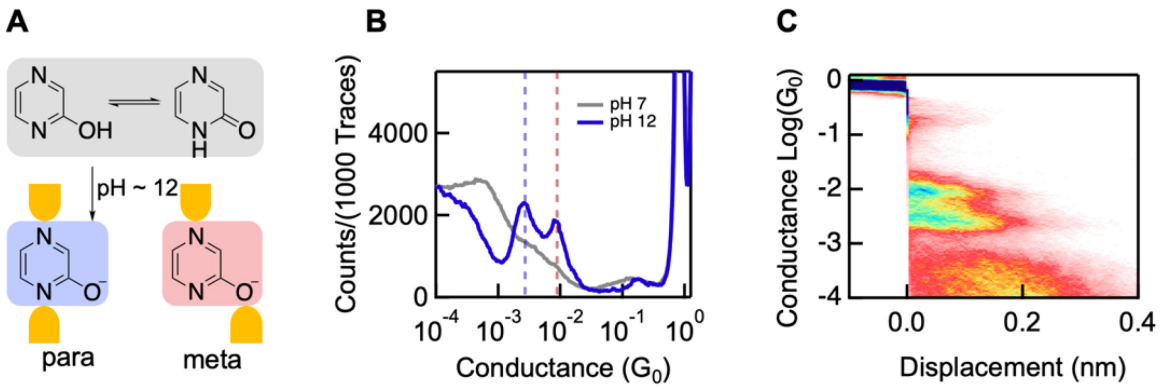

Figure 4. A) Molecular structures for OHpyz with predicted junction geometries through the para and meta pathways. B) 1D Conductance histogram of OHpyz measured in neutral conditions, pH ~ 7 (gray) and in basic conditions, pH ~ 12 (blue). C) 2D conductance histogram of OHpyz measured in basic conditions.

To summarize, the addition of the OH substituent to the meta position of the pyz ring modulates the DQI through the para channel. This synthetic modification coupled with deprotonation leads to an increase in conductance from null, or below the experimental limit of ~10^{-6} G_0 (Figure 2, green) to ~ 2.6 x 10^{-3} G_0 as indicated by the blue dashed line in Figure 4B. Accounting for transport through the meta channel (red dashed line), we observe an overall conductance increase to 8.3 x 10^{-3} G_0 for OHpyz induced by pH.[3, 47-51] This is significant for a molecule of this size (~ 4 Å), with the conductance in the *on* state approaching ~1% of a fully open quantum channel.

CONCLUSION

In this work, we demonstrate QI between σ and π molecular orbitals which leads to distinct conductance phenomena in molecular junctions. This phenomenon is only possible in molecular

junctions on the order of ~ 5 Å were transport amplitudes across both types of MOs are comparable in magnitude. We show how modification of the benzene core alone can turn off conductance through the para channel by creating conditions for σ-π DQI. These insights suggest rules for how to synthetically engineer and tune short molecular systems to achieve junctions with desired QI features. Our work shows that the σ-π interference is sensitive to slight modifications in the molecular backbone due to reordering of the frontier MOs. Since frontier orbitals dominate transport, this slight change in the relative MO energies can lead to dramatic transport shifts. Having frontier σ and π orbitals also leads to additional sensitivity of the junction to mechanical modulation, as tilting the molecule alters the relative phase change through the σ and π system at the gold links. We observe that synthetic substitution can be leveraged to tune the symmetry of the π orbitals so that they become involved in transport and modulate QI features. Finally, our work shows that ionization through external pH control is a powerful way to modulate QI in molecular junctions. We demonstrate this experimentally by tuning DQI and the corresponding conductance through the para pathway in OHpyz via pH, resulting in junctions that switch between less than 0.001 G_0 to ~ 1% G_0. This work provides a platform for *in situ* manipulation of QI for the future engineering and design of molecular switching devices

METHODS

Reagents (target molecules and solvents) were obtained commercially and used without further purification.

STMBJ Measurements

Break junction measurements were performed using a home-built STMBJ and experimental protocols established previously.[34, 35] The Au tip and substrate are brought together

forming a metallic contact. The junction is then stretched apart at 16 nm/s, while current is recorded under a constant bias of 500 mV. Measurements show steps at integer values of G_0 until the Au contact is broken, which correspond to the formation of Au contacts with integer number of Au atoms in the cross-section.[52] After the Au contact is broken a nano-gap is formed between the two Au electrodes which can interact with molecules via chemical linker groups. The measurement is repeated in the presence of target molecules in solution or deposited on the Au surface. At least 10,000 conductance traces showing the evolution of a junction as a function of displacement were compiled into histograms without data selection and normalized to enable comparison. Target molecules were dissolved in either 1,2,4-trichlorobenzene or H_2O, depending on solubility, and diluted to 1 mM concentrations. Measurements in H_2O were performed using a dropcast method as previously reported[35] or in solution using a wax-coated tip. The pH of the solution was adjusted using 1mM NaOH and 1mM HCl.

DFT Calculations

Density function theory (DFT) calculations for gas phase molecular orbitals were performed with Gaussian with PBE and B3LYP functionals and a Def2-TZVP basis set.[53-55] Transport calculations were performed with FHI-aims and AITRANS with a PBE exchange correlation functional. A light level basis set was used for initial calculations to probe all junction geometries and final geometries were calculated with a tight level basis set.[26, 56, 57] Pre-built Au(111) electrodes from the FHI-aims package were used. The Au37 electrode consists of a gold pyramid with five layers and 35 atoms with two additional Au adatoms on the sides of pyramid. The molecule was first relaxed with Au37 electrodes, frozen except for the molecule and four apex Au atoms on each electrode. The interaction (binding) energies between the electrode and molecule were calculated as the energy difference between the relaxed junction structure and the

components of the junction relaxed separately (each electrode and the pyz molecule). Transmission across the junction as a function of energy at zero bias was calculated with non-equilibrium Green's Function using AITRANSS. Each Au electrode was then moved in or out in increments of 0.05 Å and the calculations are repeated.

ASSOCIATED CONTENT

Supporting Information

The following files are available free of charge: pyzSI.doc. This material contains: additional theoretical calculations and details and additional conductance data and controls.

AUTHOR INFORMATION

Corresponding Author

* Maria Kamenetska; orcid.org/0000-0002-0390-035X; Email: mkamenet@bu.edu

Funding Sources

This work was supported by the National Science Foundation under award # 2145276.

ACKNOWLEDGEMENT:

The authors acknowledge support from the Boston University Photonics Center. HES acknowledges support from a BUnano Cross-Disciplinary Fellowship.

REFERENCES

1. Manrique, D. Z.; Huang, C.; Baghernejad, M.; Zhao, X.; Al-Owaedi, O. A.; Sadeghi, H.; Kaliginedi, V.; Hong, W.; Gulcur, M.; Wandlowski, T.; Bryce, M. R.; Lambert, C. J., A quantum circuit rule for interference effects in single-molecule electrical junctions. *Nature Communications* **2015,** *6*, 6389.
2. Gunasekaran, S.; Greenwald, J. E.; Venkataraman, L., Visualizing Quantum Interference in Molecular Junctions. *Nano Letters* **2020,** *20*, 2843-2848.
3. Greenwald, J. E.; Cameron, J.; Findlay, N. J.; Fu, T.; Gunasekaran, S.; Skabara, P. J.; Venkataraman, L., Highly nonlinear transport across single-molecule junctions via destructive quantum interference. *Nat Nanotechnol* **2021,** *16*, 313-317.
4. Liu, S.-X.; Ismael, A. K.; Al-Jobory, A.; Lambert, C. J., Signatures of Room-Temperature Quantum Interference in Molecular Junctions. *Accounts of Chemical Research* **2023,** *56*, 322-331.
5. Frisenda, R.; Janssen, V. A. E. C.; Grozema, F. C.; van der Zant, H. S. J.; Renaud, N., Mechanically controlled quantum interference in individual π-stacked dimers. *Nature Chemistry* **2016,** *8*, 1099-1104.
6. Camarasa-Gómez, M.; Hernangómez-Pérez, D.; Inkpen, M. S.; Lovat, G.; Fung, E. D.; Roy, X.; Venkataraman, L.; Evers, F., Mechanically Tunable Quantum Interference in Ferrocene-Based Single-Molecule Junctions. *Nano Letters* **2020,** *20*, 6381-6386.
7. Reznikova, K.; Hsu, C.; Schosser, W. M.; Gallego, A.; Beltako, K.; Pauly, F.; van der Zant, H. S. J.; Mayor, M., Substitution Pattern Controlled Quantum Interference in [2.2]Paracyclophane-Based Single-Molecule Junctions. *Journal of the American Chemical Society* **2021,** *143*, 13944-13951.
8. Zhu, Y.; Zhou, Y.; Ren, L.; Ye, J.; Wang, H.; Liu, X.; Huang, R.; Liu, H.; Liu, J.; Shi, J.; Gao, P.; Hong, W., Switching Quantum Interference in Single-Molecule Junctions by Mechanical Tuning. *Angewandte Chemie International Edition* **2023,** *62*, e202302693.
9. Darwish, N.; Díez-Pérez, I.; Guo, S.; Tao, N.; Gooding, J. J.; Paddon-Row, M. N., Single Molecular Switches: Electrochemical Gating of a Single Anthraquinone-Based Norbornylogous Bridge Molecule. *The Journal of Physical Chemistry C* **2012,** *116*, 21093-21097.
10. Yang, G.; Sangtarash, S.; Liu, Z.; Li, X.; Sadeghi, H.; Tan, Z.; Li, R.; Zheng, J.; Dong, X.; Liu, J.; Yang, Y.; Shi, J.; Xiao, Z.; Zhang, G.; Lambert, C.; Hong, W.; Zhang, D., Protonation tuning of quantum interference in azulene-type single-molecule junctions. *Chemical Science* **2017,** *8*, 7505-7509.
11. Lambert, C. J.; Liu, S.-X., A Magic Ratio Rule for Beginners: A Chemist's Guide to Quantum Interference in Molecules. *Chemistry – A European Journal* **2018,** *24*, 4193-4201.
12. Huang, B.; Liu, X.; Yuan, Y.; Hong, Z.-W.; Zheng, J.-F.; Pei, L.-Q.; Shao, Y.; Li, J.-F.; Zhou, X.-S.; Chen, J.-Z.; Jin, S.; Mao, B.-W., Controlling and Observing Sharp-Valleyed Quantum Interference Effect in Single Molecular Junctions. *Journal of the American Chemical Society* **2018,** *140*, 17685-17690.
13. Jiang, F.; Trupp, D. I.; Algethami, N.; Zheng, H.; He, W.; Alqorashi, A.; Zhu, C.; Tang, C.; Li, R.; Liu, J.; Sadeghi, H.; Shi, J.; Davidson, R.; Korb, M.; Sobolev, A. N.; Naher, M.; Sangtarash, S.; Low, P. J.; Hong, W.; Lambert, C. J., Turning the Tap: Conformational Control of Quantum Interference to Modulate Single-Molecule Conductance. *Angewandte Chemie International Edition* **2019,** *58*, 18987-18993.
14. Tang, C.; Huang, L.; Sangtarash, S.; Noori, M.; Sadeghi, H.; Xia, H.; Hong, W., Reversible Switching between Destructive and Constructive Quantum Interference Using

Atomically Precise Chemical Gating of Single-Molecule Junctions. *Journal of the American Chemical Society* **2021,** *143*, 9385-9392.
15. Garner, M. H.; Li, H.; Chen, Y.; Su, T. A.; Shangguan, Z.; Paley, D. W.; Liu, T.; Ng, F.; Li, H.; Xiao, S.; Nuckolls, C.; Venkataraman, L.; Solomon, G. C., Comprehensive suppression of single-molecule conductance using destructive σ-interference. *Nature* **2018,** *558*, 415-419.
16. Zhang, B.; Garner, M. H.; Li, L.; Campos, L. M.; Solomon, G. C.; Venkataraman, L., Destructive quantum interference in heterocyclic alkanes: the search for ultra-short molecular insulators. *Chemical Science* **2021,** *12*, 10299-10305.
17. Xiao; Xu; Tao, N. J., Measurement of Single Molecule Conductance: Benzenedithiol and Benzenedimethanethiol. *Nano Letters* **2004,** *4*, 267-271.
18. Quek, S. Y.; Venkataraman, L.; Choi, H. J.; Louie, S. G.; Hybertsen, M. S.; Neaton, J. B., Amine−Gold Linked Single-Molecule Circuits: Experiment and Theory. *Nano Letters* **2007,** *7*, 3477-3482.
19. Yoshizawa, K.; Tada, T.; Staykov, A., Orbital Views of the Electron Transport in Molecular Devices. *Journal of the American Chemical Society* **2008,** *130*, 9406-9413.
20. Kamenetska, M.; Quek, S. Y.; Whalley, A. C.; Steigerwald, M. L.; Choi, H. J.; Louie, S. G.; Nuckolls, C.; Hybertsen, M. S.; Neaton, J. B.; Venkataraman, L., Conductance and Geometry of Pyridine-Linked Single-Molecule Junctions. *Journal of the American Chemical Society* **2010,** *132*, 6817-6821.
21. Kaneko, S.; Takahashi, R.; Fujii, S.; Nishino, T.; Kiguchi, M., Controlling the formation process and atomic structures of single pyrazine molecular junction by tuning the strength of the metal–molecule interaction. *Physical Chemistry Chemical Physics* **2017,** *19*, 9843-9848.
22. Isshiki, Y.; Nishino, T.; Fujii, S., Electronic Structure and Transport Properties of Single-Molecule Junctions with Different Sizes of π-Conjugated System. *The Journal of Physical Chemistry C* **2021,** *125*, 3472-3479.
23. Park, Y. S.; Whalley, A. C.; Kamenetska, M.; Steigerwald, M. L.; Hybertsen, M. S.; Nuckolls, C.; Venkataraman, L., Contact Chemistry and Single-Molecule Conductance: A Comparison of Phosphines, Methyl Sulfides, and Amines. *Journal of the American Chemical Society* **2007,** *129*, 15768-15769.
24. Borges, A.; Fung, E. D.; Ng, F.; Venkataraman, L.; Solomon, G. C., Probing the Conductance of the σ-System of Bipyridine Using Destructive Interference. *The Journal of Physical Chemistry Letters* **2016,** *7*, 4825-4829.
25. Arnold, A.; Weigend, F.; Evers, F., Quantum chemistry calculations for molecules coupled to reservoirs: Formalism, implementation, and application to benzenedithiol. *The Journal of Chemical Physics* **2007,** *126*, 174101.
26. Blum, V.; Gehrke, R.; Hanke, F.; Havu, P.; Havu, V.; Ren, X.; Reuter, K.; Scheffler, M., Ab initio molecular simulations with numeric atom-centered orbitals. *Computer Physics Communications* **2009,** *180*, 2175-2196.
27. Evers, F.; Korytár, R.; Tewari, S.; van Ruitenbeek, J. M., Advances and challenges in single-molecule electron transport. *Reviews of Modern Physics* **2020,** *92*, 035001.
28. Liu, Z.-F.; Neaton, J. B., Communication: Energy-dependent resonance broadening in symmetric and asymmetric molecular junctions from an ab initio non-equilibrium Green's function approach. *The Journal of Chemical Physics* **2014,** *141*.

29. Kim, T. K.; Liu, Z.-F.; Lee, C.; Neaton, J. B.; Venkataraman, L., Charge transport and rectification in molecular junctions formed with carbon-based electrodes. *Proceesdings of the National Academy of Sciences* **2014,** *111*, 10928-10932.
30. Sangtarash, S.; Vezzoli, A.; Sadeghi, H.; Ferri, N.; O'Brien, H. M.; Grace, I.; Bouffier, L.; Higgins, S. J.; Nichols, R. J.; Lambert, C. J., Gateway state-mediated, long-range tunnelling in molecular wires. *Nanoscale* **2018,** *10*, 3060-3067.
31. Kaliginedi, V.; V. Rudnev, A.; Moreno-García, P.; Baghernejad, M.; Huang, C.; Hong, W.; Wandlowski, T., Promising anchoring groups for single-molecule conductance measurements. *Physical Chemistry Chemical Physics* **2014,** *16*, 23529-23539.
32. McNeely, J.; Miller, N.; Pan, X.; Lawson, B.; Kamenetska, M., Angstrom-Scale Ruler Using Single Molecule Conductance Signatures. *The Journal of Physical Chemistry C* **2020,** *124*, 13427-13433.
33. Fu, T.; Frommer, K.; Nuckolls, C.; Venkataraman, L., Single-Molecule Junction Formation in Break-Junction Measurements. *The Journal of Physical Chemistry Letters* **2021,** *12*, 10802-10807.
34. Kamenetska, M.; Koentopp, M.; Whalley, A. C.; Park, Y. S.; Steigerwald, M. L.; Nuckolls, C.; Hybertsen, M. S.; Venkataraman, L., Formation and Evolution of Single-Molecule Junctions. *Physical Review Letters* **2009,** *102*, 126803.
35. Pan, X.; Lawson, B.; Rustad, A. M.; Kamenetska, M., pH-Activated Single Molecule Conductance and Binding Mechanism of Imidazole on Gold. *Nano Letters* **2020,** *20*, 4687-4692.
36. Su, T. A.; Neupane, M.; Steigerwald, M. L.; Venkataraman, L.; Nuckolls, C., Chemical principles of single-molecule electronics. *Nature Reviews Materials* **2016,** *1*, 16002.
37. Hong, W.; Manrique, D. Z.; Moreno-García, P.; Gulcur, M.; Mishchenko, A.; Lambert, C. J.; Bryce, M. R.; Wandlowski, T., Single Molecular Conductance of Tolanes: Experimental and Theoretical Study on the Junction Evolution Dependent on the Anchoring Group. *Journal of the American Chemical Society* **2012,** *134*, 2292-2304.
38. Hamill, J. M.; Ismael, A.; Al-Jobory, A.; Bennett, T. L. R.; Alshahrani, M.; Wang, X.; Akers-Douglas, M.; Wilkinson, L. A.; Robinson, B. J.; Long, N. J.; Lambert, C.; Albrecht, T., Quantum Interference and Contact Effects in the Thermoelectric Performance of Anthracene-Based Molecules. *The Journal of Physical Chemistry C* **2023,** *127*, 7484-7491.
39. Skipper, H. E.; May, C. V.; Rheingold, A. L.; Doerrer, L. H.; Kamenetska, M., Hard–Soft Chemistry Design Principles for Predictive Assembly of Single Molecule-Metal Junctions. *Journal of the American Chemical Society* **2021,** *143*, 16439-16447.
40. Wu, S.; González, M. T.; Huber, R.; Grunder, S.; Mayor, M.; Schönenberger, C.; Calame, M., Molecular junctions based on aromatic coupling. *Nature Nanotechnology* **2008,** *3*, 569-574.
41. Martín, S.; Grace, I.; Bryce, M. R.; Wang, C.; Jitchati, R.; Batsanov, A. S.; Higgins, S. J.; Lambert, C. J.; Nichols, R. J., Identifying Diversity in Nanoscale Electrical Break Junctions. *Journal of the American Chemical Society* **2010,** *132*, 9157-9164.
42. Chen, F.; Li, X.; Hihath, J.; Huang, Z.; Tao, N., Effect of Anchoring Groups on Single-Molecule Conductance: Comparative Study of Thiol-, Amine-, and Carboxylic-Acid-Terminated Molecules. *Journal of the American Chemical Society* **2006,** *128*, 15874-15881.
43. Martín, S.; Haiss, W.; Higgins, S.; Cea, P.; López, M. C.; Nichols, R. J., A Comprehensive Study of the Single Molecule Conductance of α,ω-Dicarboxylic Acid-Terminated Alkanes. *The Journal of Physical Chemistry C* **2008,** *112*, 3941-3948.

44. Ahn, S.; Aradhya, S. V.; Klausen, R. S.; Capozzi, B.; Roy, X.; Steigerwald, M. L.; Nuckolls, C.; Venkataraman, L., Electronic transport and mechanical stability of carboxyl linked single-molecule junctions. *Physical Chemistry Chemical Physics* **2012,** *14*, 13841-13845.
45. Huang, J.; Grys, D.-B.; Griffiths, J.; de Nijs, B.; Kamp, M.; Lin, Q.; Baumber, J. J., Tracking interfacial single-molecule pH and binding dynamics via vibrational spectroscopy. *Science Advances* **2021,** *7*, eabg1790.
46. Huang, M.; Zhou, Q.; Liang, F.; Yu, L.; Xiao, B.; Li, Y.; Zhang, M.; Chen, Y.; He, J.; Xiao, S.; Chang, S., Detecting Individual Bond Switching within Amides in a Tunneling Junction. *Nano Letters* **2021,** *21*, 5409-5414.
47. Vazquez, H.; Skouta, R.; Schneebeli, S.; Kamenetska, M.; Breslow, R.; Venkataraman, L.; Hybertsen, M. S., Probing the conductance superposition law in single-molecule circuits with parallel paths. *Nature Nanotechnology* **2012,** *7*, 663-667.
48. Bergfield, J. P.; Heitzer, H. M.; Van Dyck, C.; Marks, T. J.; Ratner, M. A., Harnessing Quantum Interference in Molecular Dielectric Materials. *ACS Nano* **2015,** *9*, 6412-6418.
49. Yin, X.; Zang, Y.; Zhu, L.; Low, J. Z.; Liu, Z.-F.; Cui, J.; Neaton, J. B.; Venkataraman, L.; Campos, L. M., A reversible single-molecule switch based on activated antiaromaticity. *Science Advances* **2017,** *3*, eaao2615.
50. Bai, J.; Daaoub, A.; Sangtarash, S.; Li, X.; Tang, Y.; Zou, Q.; Sadeghi, H.; Liu, S.; Huang, X.; Tan, Z.; Liu, J.; Yang, Y.; Shi, J.; Mészáros, G.; Chen, W.; Lambert, C.; Hong, W., Anti-resonance features of destructive quantum interference in single-molecule thiophene junctions achieved by electrochemical gating. *Nature Materials* **2019,** *18*, 364-369.
51. Yan, Z.; Li, X.; Li, Y.; Jia, C.; Xin, N.; Li, P.; Meng, L.; Zhang, M.; Chen, L.; Yang, J.; Wang, R.; Guo, X., Single-molecule field effect and conductance switching driven by electric field and proton transfer. *Science Advances* **2022,** *8*, eabm3541.
52. Yanson, A. I.; Bollinger, G. R.; van den Brom, H. E.; Agraït, N.; van Ruitenbeek, J. M., Formation and manipulation of a metallic wire of single gold atoms. *Nature* **1998,** *395*, 783-785.
53. Perdew, J. P.; Burke, K.; Ernzerhof, M., Generalized Gradient Approximation Made Simple. *Physical Review Letters* **1996,** *77*, 3865-3868.
54. Frisch, M. J.; Trucks, G. W.; Schlegel, H. B.; Scuseria, G. E.; Robb, M. A.; Cheeseman, J. R.; Scalmani, G.; Barone, V.; Petersson, G. A.; Nakatsuji, H.; Li, X.; Caricato, M.; Marenich, A. V.; Bloino, J.; Janesko, B. G.; Gomperts, R.; Mennucci, B.; Hratchian, H. P.; Ortiz, J. V.; Izmaylov, A. F., et al. *Gaussian 16 Rev. C.01*, Wallingford, CT, 2016.
55. Weigend, F.; Ahlrichs, R., Balanced basis sets of split valence, triple zeta valence and quadruple zeta valence quality for H to Rn: Design and assessment of accuracy. *Physical Chemistry Chemical Physics* **2005,** *7*, 3297-3305.
56. Ren, X.; Rinke, P.; Blum, V.; Wieferink, J.; Tkatchenko, A.; Sanfilippo, A.; Reuter, K.; Scheffler, M., Resolution-of-identity approach to Hartree–Fock, hybrid density functionals, RPA, MP2 andGWwith numeric atom-centered orbital basis functions. *New Journal of Physics* **2012,** *14*, 053020.
57. Bagrets, A., Spin-Polarized Electron Transport Across Metal–Organic Molecules: A Density Functional Theory Approach. *Journal of Chemical Theory and Computation* **2013,** *9*, 2801-2815.